Acta Crystallographica Section A
Foundations of Crystallography
ISSN 0108-7673

Received 21 February 2000
Accepted 29 February 2000

Dedicated to Professor Vedene H. Smith on the occasion of his 65th birthday

On the origin of topological differences between experimental and theoretical crystal charge densities

Anatoliy Volkov,[a] Yuriy Abramov,[a] Philip Coppens[a]* and Carlo Gatti[b]

[a]Department of Chemistry, State University of New York at Buffalo, Buffalo, NY 14260-3000, USA, and [b]Centro CNR-CSRSRC, Department of Physical Chemistry and Electrochemistry, University of Milano, via Golgi 19, 20133 Milano, Italy. Correspondence e-mail: coppens@acsu.buffalo.edu

Topological analysis of experimental and theoretical (molecular and crystal) electron densities of *p*-nitroaniline and *p*-amino-*p*′-nitrobiphenyl reveals considerable discrepancies between experiment and theory for the bond critical points properties. Particularly large differences occur for the positive curvature along the bond path (λ_3). The differences become somewhat smaller when more extended basis sets and correlation effects are introduced in the theoretical calculations. The effect of the crystal matrix on the properties of bond critical points is evaluated for the *p*-nitroaniline molecule using the 6-21G** and 6-31G** basis sets. The differences between the isolated molecule and the molecule in the crystal are too small to explain the quantitative disagreement between the theoretical and experimental topologies reported in the literature and found in the current study. For most bonds, the observed changes in the properties of the electron density agree well for both basis sets but some discrepancies are found for changes in λ_3 for N—H and aromatic C—C bonds. When the theoretical densities are projected into the multipole density functions through refinement of the theoretical structure factors, the topological properties change and differences between theory and experiment are reduced. The main origin of the observed discrepancies is attributed to the nature of the radial functions in the experimental multipole model.

1. Introduction

The theory of atoms in molecules (AIM) (Bader, 1990) is a natural tool for deducing chemical information from the total charge density. The great advantage of such an analysis is that it can equally well be applied to experimental and theoretical densities. Owing to the advances in computer technology, fully periodic *ab initio* calculations on large systems can now be performed. Thus, it has become possible to compare directly the experimental and theoretical topology of the electron-density distribution in crystals.

Several studies of the topology of the experimental density have been reported (Gatti *et al.*, 1992; Howard *et al.*, 1995; Bianchi *et al.*, 1996, 1998; Flaig *et al.*, 1998; Koritsanszky *et al.*, 1998; Coppens *et al.*, 1999), and the observed discrepancies with theoretical calculations on isolated molecules (Gatti *et al.*, 1992; Howard *et al.*, 1995; Flaig *et al.*, 1998; Coppens *et al.*, 1999) and the periodic density (Bianchi *et al.*, 1996) have been analyzed. In the current work, comparison is made with both isolated molecule and periodic crystal theoretical densities, the experimental densities being derived from 20 K synchrotron data on *p*-nitroaniline (PNA) and *p*-amino-*p*′-nitrobiphenyl (PANB).

Abramov *et al.* (1999) have pointed out the ambiguity in the evaluation of static molecular properties, such as the dipole moment, from the aspherical atom multipole refinements of experimental X-ray diffraction data, owing to the overlap of basis functions in adjacent molecules. Space partitioning based on multipolar density functions corresponds to a 'fuzzy boundary' partitioning scheme, which leads to non-locality of the charge density assigned to each center (Coppens, 1997). To reduce the effect of overlap of the basis functions in the charge-density refinement, a κ'-restricted model was introduced in which information from the periodic Hartree–Fock (PHF) calculation is used to define the radial part of deformation functions (Volkov, Abramov & Coppens, 2000). The need for a κ'-restricted model (KRMM) is strongly supported by a recently published study on NaH_2PO_4, in which it is shown that different values of κ' for the P atom give identical agreement factors but strongly affect the value of the Laplacian at the P—O bond critical point (Pérès *et al.*, 1999). The KRMM model results are included in the testing presented in this paper.

2. Experimental data

Accurate 20 K X-ray data for both PNA (Fig. 1*a*) and PANB (Fig. 1*b*) were collected at the SUNY X3A1 beamline at the National Synchrotron Light Source (wavelength 0.643 Å), using a Bruker Smart 1000 CCD area detector and a closed-cycle helium Displex CT211 cryostat. Details of the data collection and processing have been published elsewhere (Volkov *et al.*, 1999; Coppens *et al.*, 2000). Structurally, the packing arrangements of PNA and PANB are very similar; both crystals contain sheets of N—O···H—N hydrogen-bonded molecules, oriented perpendicular to the [101] and [001] directions in PNA and PANB, respectively, with each molecule being hydrogen-bonded to four other molecules. However, PANB crystallizes in a noncentrosymmetric space group ($Pca2_1$), while the space group of PNA ($P2_1/n$) is centrosymmetric.

Aspherical atom refinements were carried out with the *XD* package (Koritsanszky *et al.*, 1997) using the Hansen–Coppens multipole formalism (Coppens, 1997). The formalism describes the static electron density in the crystal by a superposition of aspherical *pseudoatoms*, the charge density of which is modeled by a nucleus-centered multipole expansion

$$\rho_k(\mathbf{r}) = P_c\rho_c(r) + P_v\kappa^3\rho_v(\kappa r) + \kappa'^3\sum_{l=1}^{4} R_l(\kappa' r)\sum_{m=1}^{l} P_{lm\pm}d_{lm\pm}(\mathbf{r}/r),$$

where ρ_c and ρ_v are spherically averaged free-atom Hartree–Fock core and valence densities normalized to one electron; $d_{lm\pm}$ are real spherical harmonic angular functions; R_l are normalized Slater-type radial functions, including a factor r^n, with $n = 2, 2, 3$ for the dipolar, quadrupolar and octupolar deformation terms, respectively. κ and κ' are dimensionless expansion–contraction parameters, which can be refined in the fitting procedure along with the populations P_v and $P_{lm\pm}$. HF densities are used for the spherically averaged core (ρ_c) and valence (ρ_v) shells. The default conventional sets of R_l functions were used for all pseudoatoms (Coppens, 1997). The κ and κ' parameters of the hydrogen atoms were fixed at a value of 1.2 throughout all refinements. In order to reduce the number of parameters for both PNA and PANB, the multipole coefficients of the non-hydrogen atoms were constrained to obey local mirror-plane symmetry (m), the mirror plane being defined as the plane through the atom and two adjacent atoms, while H atoms were given cylindrical symmetry. Additional constraints corresponding to the (mm) symmetry were imposed on atoms located on the long axis of the molecules. All chemical constraints were justified by examination of the final residual density maps. A molecular electroneutrality constraint was applied in all refinements.

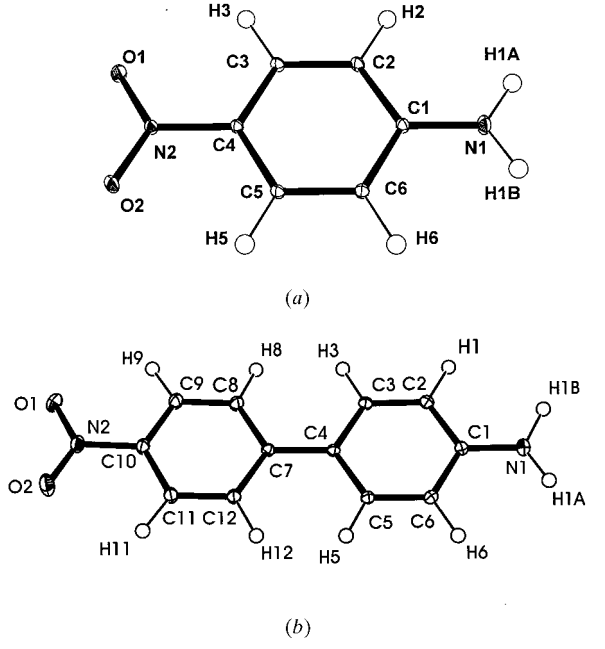

Figure 1
Molecular structures of (*a*) *p*-nitroaniline (PNA) and (*b*) *p*-amino-*p*′-nitrobiphenyl (PANB).

Table 1
Summary of multipole refinements of experimental and theoretical data for PNA and PANB.

	PNA		PANB	
	KRMM	UMM	KRMM	UMM
Experimental X-ray data				
N_{ref}/N_{par}	19.0	18.2	15.5	14.9
R_F (%)	1.54	1.51	1.70	1.69
Theoretical structure factors				
N_{ref}/N_{par}	–	75.4	–	48.4
R_F (%)	–	0.75	–	0.76

In the multipole refinements, the procedure recently described by Abramov *et al.* (1999) was followed. In the first stage, high-order refinements ($\sin\theta/\lambda > 0.7$ Å^{-1}) were performed to determine unbiased positional and thermal parameters for the non-hydrogen atoms. Hydrogen positions were obtained by extending X—H distances to their standard neutron diffraction values ($C_{aromatic}$—H = 1.083 Å and N_{amino}—H = 1.010 Å) (*International Tables for Crystallography*, 1992). These distances were kept constant in subsequent refinements. In the next stage, a κ refinement ($P_{lm\pm} = 0$) was performed with all structural parameters, except the isotropic thermal parameters of the H atoms, being fixed at the previously refined values. In the final refinement, both standard unrestricted (UMM) and κ'-restricted multipole refinements were carried out. In the UMM refinement, all structural and electronic (P_v, $P_{lm\pm}$, κ and κ') parameters are refined, while, in KRMM, the κ' parameters are fixed at values derived from multipole refinements of theoretical structure factors on a number of compounds using periodic Hartree–Fock (PHF) calculations at the 6-21G** level (Volkov, Abramov & Coppens, 2000).[1] This approach imposes an additional locality constraint on the atomic charge distribution, which results in more consistent representation of molecular dipole moments and superior deformation-density

[1] Values of κ' used in this study are: O 1.12; N(amino) 0.94; N(nitro) 0.82; C(H) 0.94; C(CCC) 0.96; C(CCN) 0.92.

Table 2
Effect of basis-set selection on the topology of the theoretical isolated molecule density of PNA.

				Hessian eigenvalues (e Å^{-5})			
	Δ_{BCP} (Å)†	ρ (e Å^{-3})	$\nabla^2\rho$ (e Å^{-5})	λ_1	λ_2	λ_3	ε
O—N							
HF/6-21G**	0.039	3.36	−36.1	−31.9	−27.8	23.6	0.15
HF/6-31G**	0.011	3.36	−26.3	−30.3	−26.9	31.0	0.12
HF/6-311G**	0.016	3.42	−29.9	−32.5	−28.9	31.5	0.13
HF/cc-pVTZ‡	0.018	3.46	−31.3	−34.5	−30.3	33.5	0.14
N_{amino}—C							
HF/6-21G**	0.208	2.15	−16.5	−17.6	−17.2	18.3	0.02
HF/6-31G**	0.233	2.19	−18.2	−17.8	−17.2	16.9	0.03
HF/6-311G**	0.220	2.17	−18.6	−16.9	−16.5	14.8	0.03
HF/cc-pVTZ	0.219	2.23	−22.4	−18.7	−18.3	14.6	0.02
N_{nitro}—C							
HF/6-21G**	0.233	1.84	−10.4	−14.0	−11.6	15.2	0.20
HF/6-31G**	0.266	1.84	−7.8	−13.5	−10.8	16.6	0.25
HF/6-311G**	0.260	1.83	−6.7	−12.8	−10.3	16.4	0.25
HF/cc-pVTZ	0.255	1.87	−11.7	−14.5	−11.4	14.1	0.28
Aromatic C—C parallel to molecular axis							
HF/6-21G**	0.094	2.26	−29.2	−17.6	−13.6	2.0	0.30
HF/6-31G**	0.017	2.21	−24.0	−17.0	−13.1	5.9	0.30
HF/6-311G**	0.021	2.19	−24.5	−16.8	−13.1	5.4	0.28
HF/cc-pVTZ	0.027	2.28	−29.6	−18.7	−14.8	3.9	0.26
N—H							
HF/6-21G**	0.243	2.34	−42.1	−33.4	−31.2	22.4	0.07
HF/6-31G**	0.265	2.34	−46.0	−32.6	−30.7	17.4	0.06
HF/6-311G**	0.247	2.30	−42.7	−31.6	−29.5	18.4	0.07
HF/cc-pVTZ	0.259	2.36	−49.8	−34.1	−32.3	16.5	0.06
C—H							
HF/6-21G**	0.132	1.99	−28.0	−18.0	−17.3	7.2	0.04
HF/6-31G**	0.121	1.97	−26.8	−18.2	−17.5	8.9	0.04
HF/6-311G**	0.144	1.94	−25.4	−18.2	−17.5	10.2	0.04
HF/cc-pVTZ	0.145	2.02	−30.2	−19.9	−19.3	9.0	0.03

† Δ_{BCP} is defined to be positive when the critical point is displaced from the bond midpoint towards the second atom. ‡ Dunning's correlation consistent valence triple-zeta + polarization basis set (Woon & Dunning, 1993).

maps. The multipole expansion was truncated at the octupole level ($l_{max} = 3$) for the non-hydrogen atoms and at the quadrupole level ($l_{max} = 2$) for the H atoms. No significant correlations were found between the quadrupole parameters on the H atoms and the temperature parameters. A summary of the multipole refinements of experimental data for both PNA and PANB is given in Table 1.

The topological analysis of the experimental electron density was carried out with the *XD* package (Koritsanszky *et al.* 1997).

3. Theoretical calculations

Ab initio single-molecule and crystal calculations for PNA and PANB were performed at the Hartree–Fock level using the programs *Gaussian94* (Frisch *et al.*, 1995) and *CRYSTAL98* (Saunders *et al.*, 1998), respectively. Molecular and crystal geometries were taken from the experimental X-ray KRMM refinements. All calculations were performed at the Center for Computational Research at SUNY at Buffalo using a 64-processor Silicon Graphics Origin2000 supercomputer and a 62-node Sun Ultra 5 Beowulf cluster.

Single-molecule calculations were carried out at Hartree–Fock, density-functional (DFT) and second-order Møller–Plesset perturbation theory (Møller & Plesset, 1934) (MP2) levels. DFT calculations were performed using Becke's three-parameter hybrid method (Becke, 1993) combined with the non-local correlation functional of Lee *et al.* (1988) (B3LYP keyword in *Gaussian94*). In all isolated molecule calculations, the standard molecular split valence 6-21G**, 6-31G**, 6-311G** and cc-pVTZ basis sets were used. Fully periodic calculations were performed only at the Hartree–Fock level (PHF) using two types of basis set. The first is the standard molecular 6-21G** basis set, which has been successfully tested on the crystal structure of urea (Dovesi *et al.*, 1990). The second basis set, 6-31G**, has previously been used for PHF calculations of crystalline HCN (Platts & Howard, 1996), ice VIII (Ojamae *et al.*, 1994) and urea (Gatti *et al.*, 1994). In order to avoid severe numerical instabilities in periodic calculations with the 6-31G** set, the diffuse outermost Gaussian functions of hydrogen and carbon atoms were scaled [the expo-

nents were changed from 0.16127780 (H) and 0.1687144 (C) to 0.2 Bohr^{-1} for both atoms] in the calculations of the crystal and for comparison purposes also for the molecule in the crystal geometry (Towler, 1999). In the periodic calculations, the shrinking factor for the Monkhorst net (Monkhorst & Pack, 1976) was set equal to 14 and 12 for PNA and PANB, respectively. This produced 512 and 518 k points in the irreducible part of the Brillouin zone, respectively. Analysis of theoretical electron density was performed with the programs *AIMPAC* (Biegler-König *et al.*, 1982) and *TOPOND98* (Gatti, 1999) for single-molecule and periodic calculations, respectively.

3.1. Multipole refinements of theoretical X-ray structure factors

Static crystal structure factors are obtained through Fourier transform of the ground-state charge density. For both PNA and PANB compounds, static structure factors were generated from PHF/6-21G** and PHF/6-31G** calculations. To simulate the experimental data, reflections within the range $0 < \sin\theta/\lambda < 1.05$ Å^{-1} were included. All multipole refinements were carried out with the *XD* program and based on *F*, as in the case of experimental structure factors. Although in the *ab initio* calculations the crystal density was obtained as a product of atomic Gaussian-type orbitals, in the multipole refinements we used scattering factors derived from Clementi–Roetti atomic functions (Clementi & Roetti, 1974). Stewart has shown that the difference in the radial scattering factors between Clementi orbital products and the corresponding expansion over five Gaussian-type orbitals (basically, the STO-5G basis set) is well under 1% (Stewart, 1969). Much better agreement is obviously achieved for split valence basis sets. Since all our theoretical calculations used basis sets of much higher quality than STO-5G (*i.e.* 6-21G** and 6-31G**), the difference in scattering factors should be negligible. As in refinements of experimental data, the Hansen–Coppens multipole formalism was applied but atomic temperature parameters were not refined with the static data and all positional parameters were fixed. Only unrestricted multipole refinements (UMM) were carried out using the same local symmetry and chemical constraints as in the corresponding

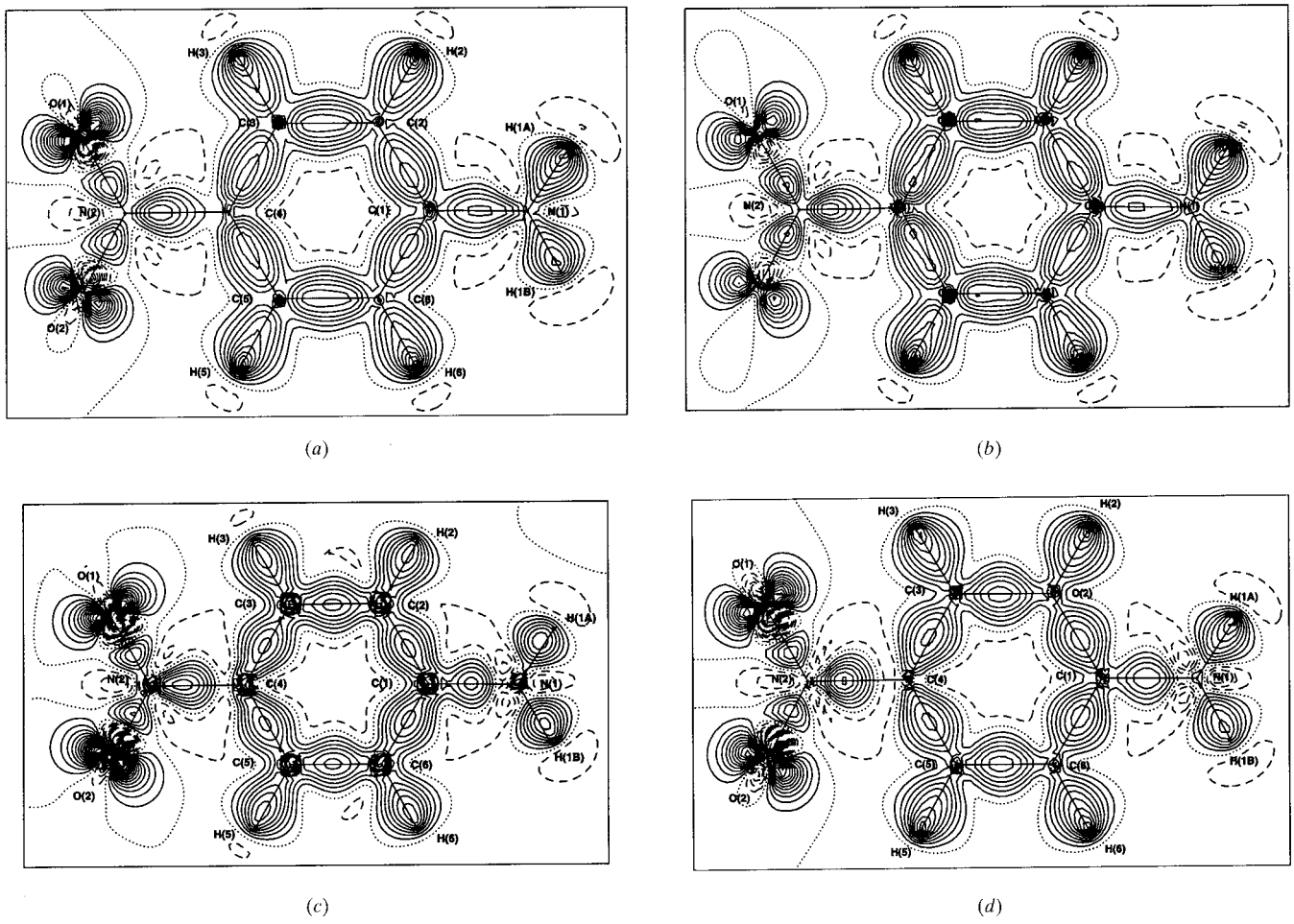

Figure 2
Theoretical and experimental deformation density maps in the plane of atoms C(3)—C(5)—C(6) in the PNA molecule. (*a*) KRMM refinement and (*b*) UMM refinement of experimental structure factors; (*c*) theoretical PHF/6-31G** deformation density; (*d*) deformation density after multipole refinement of the theoretical PHF/6-31G** structure factors. Positive, negative and zero contours are represented by solid, dashed and dotted lines, respectively. Contour intervals at 0.1 e Å^{-3}.

Table 3
Effect of electron correlation on the topology of the theoretical isolated molecule density of PNA.

	Δ_{BCP} (Å)	ρ (e Å^{-3})	$\nabla^2\rho$ (e Å^{-5})	Hessian eigenvalues (e Å^{-5})			ε
				λ_1	λ_2	λ_3	
O—N							
HF/6-311G**	0.016	3.42	−29.9	−32.5	−28.9	31.5	0.13
B3LYP/6-311G**	0.027	3.30	−23.7	−31.0	−28.0	35.3	0.11
MP2/6-311G**	0.036	3.27	−23.2	−30.3	−26.9	34.0	0.13
N_{amino}—C							
HF/6-311G**	0.220	2.17	−18.6	−16.9	−16.5	14.8	0.03
B3LYP/6-311G**	0.183	2.13	−20.7	−15.9	−14.9	10.0	0.07
MP2/6-311G**	0.199	2.11	−18.7	−15.4	−14.3	11.1	0.08
N_{nitro}—C							
HF/6-311G**	0.260	1.83	−6.7	−12.8	−10.3	16.4	0.25
B3LYP/6-311G**	0.191	1.86	−17.0	−13.5	−11.4	7.9	0.18
MP2/6-311G**	0.202	1.86	−17.4	−13.1	−11.6	7.2	0.13
Aromatic C—C parallel to molecular axis							
HF/6-311G**	0.021	2.19	−24.5	−16.8	−13.1	5.4	0.28
B3LYP/6-311G**	0.005	2.12	−21.3	−15.9	−12.9	7.6	0.23
MP2/6-311G**	−0.003	2.10	−21.1	−15.6	−12.6	6.9	0.24
N—H							
HF/6-311G**	0.247	2.30	−42.7	−31.6	−29.5	18.4	0.07
B3LYP/6-311G**	0.235	2.27	−38.3	−30.7	−28.9	21.3	0.06
MP2/6-311G**	0.242	2.25	−39.2	−30.5	−28.6	19.9	0.07
C—H							
HF/6-311G**	0.144	1.94	−25.4	−18.2	−17.5	10.2	0.04
B3LYP/6-311G**	0.148	1.90	−23.3	−18.1	−17.5	12.3	0.03
MP2/6-311G**	0.152	1.89	−23.4	−17.7	−17.3	11.6	0.02

multipole refinements of the experimental structure factors. A summary of multipole refinements of theoretical data for both PNA and PANB crystals is given in Table 1. The deformation density model in the plane of the phenyl ring of PNA, directly from the theoretical calculation and projected into the multipole model, is compared with experimental maps in Fig. 2.

4. Results and discussion

Discrepancies between the topology from the experimental density and that from theory found in the many studies cited above have been attributed to various effects. These include (i) inadequacy of the theoretical basis set; (ii) neglect of electron correlation in the theoretical calculations; (iii) the effect of the crystal lattice, as most of the theoretical calculations were performed for isolated molecules only; and (iv) limited flexibility of the basis functions employed in the multipole refinements.

Each of these will be discussed in view of the results summarized in Tables 2–5. In Table 5, results for chemically related bonds in PNA and PANB, which generally show excellent agreement, have been averaged.

(i) *Basis-set dependence* (Table 2). Several basis sets have been tested for each level of theory (*i.e.* HF, DFT and MP2). As the effect of the basis set was similar for different levels of theory, only those for the HF calculations are presented in Table 2. Examination of Table 2 shows the basis-set dependence to be different for different bond types. In general, the 6-21G** results are the outliers when large deviations occur. Considerable differences are found for Δ_{BCP} and λ_3, which are respectively the distance of the (3, −1) critical point from the bond midpoint and the curvature of the electron density along the bond path. For the O—N bond, both λ_3 and Δ_{BCP} increase, while they both decrease for N—C upon improvement of the basis set beyond 6-31G**.

(ii) *Electron correlation* (Table 3). Though the amount of electron correlation included in our calculations is quite limited and less than that in previous calculations on smaller systems (Gatti *et al.*, 1988), some general conclusions can be drawn. The density at the critical point, ρ_{BCP}, generally decreases with inclusion of correlation, except for N_{nitro}—C, for which the dependence is minor. As far as the curvature along the bond path is concerned, the N—C bonds behave differently from the other bonds, for which the curvature increases, while it is drastically reduced for N—C upon inclusion of correlation effects. A qualitatively similar result has been obtained for the C—C and $N(H_3)$—C bonds in L-alanine (Gatti *et al.*, 1992). The change is accompanied by a significant shift of the position of the BCP towards the N atom, which is as large as 0.06 Å for N_{nitro}—C. For this bond, ε decreases, indicating a reduction in π character upon inclusion of correlation effects.

(iii) *The effect of the crystal lattice* (Table 4). The effect of the crystal lattice on the topological parameters is surprisingly small in view of the well established effect of the polarizing matrix on the molecular electrostatic moments (Abramov *et*

Table 4
Effect of the crystal lattice on the properties of BCPs in the PNA molecule according to HF calculations.

Values for an isolated molecule are subtracted from those in the crystal.† Rows represent 6-21G** (1) and 6-31G** (2) basis sets. *Italic font* marks the opposite changes for 6-21G** and 6-31G** basis sets. Units of all parameters as in previous tables.

Bond A—B	R_{A-B} (Å)	Δ_{BCP}	$\Delta(\rho)$	$\Delta(\nabla^2\rho)$	$\Delta(\lambda_1)$	$\Delta(\lambda_2)$	$\Delta(\lambda_3)$	$\Delta(\varepsilon)$
O—N_{nitro}	1.234, 1.241	0.004	−0.003	−0.5	−0.1	−0.3	−0.1	0.00
		0.003	−0.002	−0.8	−0.2	−0.2	−0.4	0.00
N_{amino}—C	1.357	−0.005	0.026	−1.4	−0.3	−0.1	−1.0	*+0.01*
		−0.005	0.034	−3.2	−0.1	−0.4	−2.7	*−0.02*
N_{nitro}—C	1.435	0.008	−0.053	3.6	0.8	1.3	1.5	0.08
		0.005	−0.053	4.9	0.8	1.4	2.7	0.10
C1—C2,	1.416, 1.416	0.000	0.006	−0.2	0.0	−0.2	0.0	−0.02
C1—C6		−0.001	0.007	−0.3	−0.1	−0.3	0.0	−0.02
C2—C3,	1.383, 1.381	−0.024	−0.010	1.3	0.1	0.2	*+0.9*	0.02
C6—C5		−0.009	−0.005	0.2	0.1	0.2	*−0.1*	0.02
C4—C3,	1.400, 1.400	0.021	−0.005	*+0.5*	0.1	−0.1	*+0.5*	−0.02
C4—C5		0.007	−0.002	*−0.1*	0.1	0.0	*−0.1*	−0.02
N—H	1.010	0.011	0.003	−3.5	−1.1	−1.4	*−1.0*	−0.01
		0.011	0.003	−0.7	−1.3	−1.5	*+2.1*	−0.01
C2—H2,	1.080	0.012	0.022	−0.4	−0.6	−0.6	0.9	0.00
C6—H6		0.011	0.023	−0.8	−0.5	−0.6	0.3	0.00
C3—H3,	1.080	0.002	0.008	−0.1	−0.2	−0.2	0.2	0.00
C5—H5		0.003	0.010	−0.3	−0.2	−0.2	0.0	0.00

† In the calculations of the molecules, the basis-set superposition error (BSSE) was corrected by placing ghost orbitals on all atoms of the surrounding molecules in the crystal structure within 3.5 Å (Boys & Bernardi, 1970).

al., 1999; Gatti *et al.*, 1994; Zhang & Coppens, 1999). Though there are differences between the 6-21G** and 6-31G** results listed in Table 4, the trends predicted are the same, with the few exceptions marked in italic.

The most sensitive bonds are N—C and N—H, which is probably a result of hydrogen bonding. On the other hand, the more rigid larger curvature N—O bond, also involved in hydrogen bonding, is less affected. For N—H and N_{amino}—C, the changes are very similar to those previously found for urea (Gatti *et al.*, 1994). The curvature along the bond path decreases with hydrogen bonding for N_{amino}—C, while the density increases. The curvature for N—H increases with the better basis set. A detailed discussion can be found in the report on the urea study. For N_{nitro}—C, on the other hand, the curvature increases and the density decreases. This opposite behavior may be related to the fact that the nitro group and amino groups fulfil opposite functions in the hydrogen bond.

(iv) *The effect of the model*. Table 5 is a comparison of the topological parameters from multipole refinement of both the experimental structure factors and those directly derived from the theoretical density. In the last two rows of each entry, the results of the multipole refinement of the theoretical structure factors for both basis sets are listed. When experiment is directly compared with theory, large discrepancies are observed for λ_3, which is lower for theory in all cases, except for the N—C bonds. The theoretical curvatures are two or more times smaller than the experimental ones for O—N, C—C and C—H. Very similar results for N—O and C—H have been reported in the topological study of $Li[N(CH_3)_4]_2$-$[Co(NO_2)]_6$ (Bianchi *et al.*, 1996). A modest increase is observed for the N—C bonds. As λ_1 and λ_2 are similar for theory and experiment, the differences in λ_3 are also reflected in the $\nabla^2\rho$ values. The differences in ρ_{BCP} are small (less than 5% and ~0.1 e Å^{-3}) and often opposite to those in the curvature along the bond path. For N—C, there are drastic discrepancies in the positions of the BCP's, the theoretical BCP's being displaced towards the less electronegative C atom. The UMM and KRMM models give rather similar results, with the latter method leading to a slight decrease in curvature along the bond path. The KRMM deformation density (Fig. 2*a*) also shows a qualitatively better agreement with the theoretical deformation density (Fig. 2*c*).

When the theoretical densities are projected into the multipole model through refinement of the theoretical structure factors (Howard *et al.*, 1995), quite different results are obtained. For N—C, the agreement for λ_3 is worsened, while it is significantly improved for all other bonds. The effect of the model is qualitatively evident by examination of the theoretical deformation densities before (Fig. 2*c*) and after the multipole refinement (Fig. 2*d*). It is clear that the model as applied here biases the theoretical results.

It is interesting that discrepancies between the 6-21G** and 6-31G** theoretical results are considerably reduced by the projection into the multipole basis set. This is evident, for instance, for the positions of the critical points and for λ_3 of O—N and C—C.

Although the effects of basis-set choice and electron correlation in the theoretical calculations are important, they cannot account for the differences between the theoretical and experimental topologies. For instance, excluding the 6-21G** basis set, the combined effect of the basis-set choice and correlation on λ_3 is largest at 5 e Å^{-5} for O—N. Including such a correction in the PHF/6-31G** values reduces the discrepancy by about 40%. In other cases, the basis-set and correlation effects increase the discrepancies. Therefore, correlation and basis-set inadequacies must be discarded as an

Table 5
Effect of the model on the topology of experimental and theoretical densities of PNA and PANB.

Chemically related bonds, which generally show excellent agreement, have been averaged.

				Hessian eigenvalues (e Å^{-5})			
	Δ_{BCP} (Å)	ρ (e Å^{-3})	$\nabla^2\rho$ (e Å^{-5})	λ_1	λ_2	λ_3	ε
O—N							
X-ray/UMM	0.005	3.32	−6.6	−30.0	−27.0	50.4	0.11
X-ray/KRMM	0.012	3.31	−10.6	−29.3	−26.3	45.0	0.11
PHF/6-21G**	0.043	3.35	−35.1	−31.9	−28.0	23.8	0.14
PHF/6-31G**	0.013	3.35	−26.7	−30.3	−27.1	30.7	0.12
PHF/6-21G**/UMM	0.004	3.20	−12.4	−27.1	−25.0	39.8	0.09
PHF/6-31G**/UMM	0.001	3.26	−13.8	−27.6	−25.7	39.7	0.10
N_{amino}—C							
X-ray/UMM	0.104	2.24	−20.5	−18.6	−16.0	14.2	0.16
X-ray/KRMM	0.125	2.22	−21.1	−17.8	−15.2	11.9	0.17
PHF/6-21G**	0.203	2.16	−18.0	−17.6	−17.0	16.6	0.03
PHF/6-31G**	0.228	2.20	−21.9	−17.6	−17.3	13.2	0.02
PHF/6-21G**/UMM	0.123	2.20	−24.1	−18.3	−15.4	9.6	0.19
PHF/6-31G**/UMM	0.132	2.18	−24.6	−17.3	−15.3	7.9	0.13
N_{nitro}—C							
X-ray/UMM	0.134	1.85	−12.7	−14.7	−11.6	13.6	0.27
X-ray/KRMM	0.138	1.83	−12.9	−14.3	−11.4	12.8	0.25
PHF/6-21G**	0.242	1.75	−7.4	−12.7	−10.5	15.8	0.21
PHF/6-31G**	0.271	1.77	−4.8	−12.4	−9.8	17.4	0.27
PHF/6-21G**/UMM	0.214	1.76	−13.5	−12.7	−9.2	8.4	0.37
PHF/6-31G**/UMM	0.235	1.72	−10.2	−11.4	−8.5	9.7	0.35
Aromatic C—C parallel to molecular axis							
X-ray/UMM	0.014	2.17	−18.3	−17.0	−13.7	12.4	0.24
X-ray/KRMM	0.010	2.18	−18.6	−16.8	−13.6	11.7	0.24
PHF/6-21G**	0.101	2.23	−28.5	−17.3	−13.6	2.7	0.27
PHF/6-31G**	0.021	2.18	−23.6	−16.6	−13.0	5.9	0.28
PHF/6-21G**/UMM	0.013	2.17	−21.4	−17.1	−13.2	8.9	0.29
PHF/6-31G**/UMM	0.019	2.16	−20.7	−15.8	−12.7	8.1	0.24
N—H							
X-ray/UMM	0.22	2.32	−32.6	−30.4	−28.1	26.0	0.08
X-ray/KRMM	0.23	2.33	−32.1	−30.8	−28.7	27.4	0.08
PHF/6-21G**	0.25	2.35	−45.5	−34.5	−32.6	21.5	0.06
PHF/6-31G**	0.28	2.34	−46.5	−33.8	−32.0	19.3	0.06
PHF/6-21G**/UMM	0.23	2.25	−29.3	−29.6	−27.1	27.3	0.10
PHF/6-31G**/UMM	0.23	2.25	−28.1	−29.1	−26.7	27.8	0.09
C—H							
X-ray/UMM	0.15	1.89	−18.0	−18.0	−17.0	17.0	0.07
X-ray/KRMM	0.16	1.87	−18.0	−17.9	−16.8	16.8	0.06
PHF/6-21G**	0.14	2.01	−28.3	−18.6	−17.9	8.2	0.04
PHF/6-31G**	0.13	1.99	−27.4	−18.7	−18.0	9.2	0.04
PHF/6-21G**/UMM	0.16	1.92	−20.7	−18.6	−17.2	15.1	0.08
PHF/6-31G**/UMM	0.15	1.93	−21.1	−18.1	−16.9	13.9	0.07

explanation for the discrepancies between theory and experiment, provided good-quality basis sets are used in the calculations. Neither do the relatively small effects that occur upon incorporation of the molecule in the crystal provide an adequate explanation for the discrepancies between theory and experiment observed in previous studies, in which the crystal field was not considered.

The most striking effect evident in Table 5 is the influence of the multipole model on the theoretical densities. For O—N, the increase in the theoretical λ_3 values is 9 e Å^{-5} and, combined with the 5 e Å^{-5} basis-set/correlation correction, accounts almost completely for the observed discrepancy. For the other bonds, with the exception of N—C, a similar increase in λ_3 is observed, although the increase does not eliminate the observed discrepancy between theory and experiment when the basis set and correlation corrections are added. For N—C, the effect is opposite and, in addition, the ellipticity is considerably increased by the model analysis. This and other differences between the theoretical density before and after the model refinement indicate the need for a close examination of the radial functions used in the refinement of accurate X-ray structure factors.

5. Conclusions

In this work, we have presented a comprehensive topological analysis including the effects of basis-set size, correlation, the crystal lattice and the multipolar model on the electron

density. Comparison of the primary theoretical density with the density from a theoretical structure-factor refinement shows that the model biases the topological results. On the other hand, when applied to the 6-21G** density, the model can correct for some of the shortcomings of the less flexible basis set, as the differences between the 6-21G** and the 6-31G** results are reduced. Use of the κ' restricted model (KRMM), which is especially effective for the peripheral oxygen atoms, reduces the large discrepancies in the N—O bonds. Our analysis is limited to the Coppens–Hansen formalism with n in r^n equal to 2, 2, 3 for dipoles, quadrupoles and octupoles, respectively. However, similar conclusions regarding the model were reached in a previous study (Bianchi *et al.*, 1996), in which the *VALRAY* formalism (Stewart, 1976) was used, comparing the experimental density with the density from 3-21G *CRYSTAL92* calculations. The current work puts these conclusions on a firmer basis by including the refinement of theoretical structure factors and by eliminating the effects of correlation, the size of the basis set and the crystalline environment as the source of the discrepancies.

The 6-21G** and 6-31G** basis sets (the latter with the contraction of the outer Gaussian orbital) give very similar results for the effect of the crystal field. The less flexible set may thus be adequate for the study of the effect of the crystalline environment on the electron density (Volkov & Coppens, 2000; Volkov, Gatti *et al.*, 2000).

Topological analysis has been shown to be an effective tool for the assessment of the adequacy of the radial basis functions used. We have recently applied the AIM analysis to the study of atomic and molecular moments of the density described by the Hansen–Coppens model and similarly found a bias introduced by the multipole model when applied to the primary theoretical density (Volkov, Gatti *et al.*, 2000).

In future work, topological analysis will be used as a diagnostic tool for the improvement of the multipole-model radial functions. Such an analysis may require theoretical basis sets beyond those employed in the current study.

We would like to thank Dr Matthew D. Jones for his help at the computational stage of this work. Support of this work by the National Science Foundation (CHE9615586) and the US Department of Energy (DE-FG02-86ER45231) is gratefully acknowledged. All theoretical calculations were performed at the Center for Computational Research at SUNY at Buffalo, which is supported by grant DBI9871132 from the National Science Foundation.

References

Abramov, Yu. A., Volkov, A. & Coppens, P. (1999). *Chem. Phys. Lett.* **31**, 81–86.
Bader, R. F. (1990). *Atoms in Molecules: a Quantum Theory.* Oxford: Clarendon Press.
Becke, A. D. (1993). *J. Chem. Phys.* **98**, 5648–5652.
Bianchi, R., Gatti, C., Adovasio, V. & Nardelli, M. (1996). *Acta Cryst.* B**52**, 471–478.
Bianchi, R., Gervasio, G. & Viscardi, G. (1998). *Acta Cryst.* B**54**, 66–72.
Biegler-König, F. W., Bader, R. F. & Tang, T.-H. (1982). *J. Comput. Chem.* **13**, 317–328.
Boys, S. F. & Bernardi, F. (1970). *Mol. Phys*. **19**, 553–566.
Clementi, E. & Roetti, C. (1974). *At. Data Nucl. Data Tables*, **14**, 177–478.
Coppens, P. (1997). *X-ray Charge Densities and Chemical Bonding.* New York: Oxford University Press.
Coppens, P., Abramov, Yu., Carducci, M., Korjov, B., Novozhilova, I., Alhambra, C. & Pressprich, M. R. J. (1999). *J. Am. Chem. Soc.* **121**, 2585–2593.
Coppens, P., Wu, G., Volkov, A., Abramov, Y., Zhang, Y., Fullagar, W. K. & Ribaud, L. (2000). *Trans. Am. Crystallogr. Assoc.* In the press.
Dovesi, R., Causà, M., Orlando, R., Roetti, C. & Saunders, V. R. (1990). *J. Chem. Phys.* **12**, 7402–7411.
Flaig, R., Koritsanszky, T., Zobel, D. & Luger, P. (1998). *J. Am. Chem. Soc.* **120**, 2227–2238.
Frisch, M. J., Trucks, G. W., Schlegel, H. B., Gill, P. M., Johnson, B. G., Robb, M. A., Cheeseman, J. R., Keith, T., Petersson, G. A., Montgomery, J. A., Raghavachari, K., Al-Laham, M. A., Zakrzewski, V. G., Ortiz, J. V., Foresman, J. B., Cioslowski, J., Stefanov, B. B., Nanayakkara, A., Challacombe, M., Peng, C. Y., Ayala, P. Y., Chen, W., Wong, M. W., Andres, J. L., Replogle, E. S., Gomperts, R., Martin, R. L., Fox, D. J., Binkley, J. S., Defrees, D. J., Baker, J., Stewart, J. P., Head-Gordon, M., Gonzalez, C. & Pople, J. A. (1995). *Gaussian 94, Revision E.2.* Gaussian Inc., Pittsburgh, PA, USA.
Gatti, C. (1999). *TOPOND98 Users' Manual.* CNR-CSRSRC, Milano, Italy.
Gatti, C., Bianchi, R., Destro, R. & Merati, F. (1992). *J. Mol. Struct. (Theochem.)*, **255**, 409–433.
Gatti, C., MacDougall, P. J. & Bader, R. F. W. (1988). *J. Chem. Phys.* **88**, 3792–3804.
Gatti, C., Saunders, V. R. & Roetti, C. (1994). *J. Chem. Phys.* **101**, 10686–10696.
Howard, S. T., Hursthouse, M. B., Lehmann, C. W. & Poyner, E. A. (1995). *Acta Cryst.* B**51**, 328–337.
International Tables for Crystallography (1992). Vol. C, edited by A. J. C. Wilson. Dordrecht: Kluwer Academic Publishers.
Koritsanszky, T., Flaig, R., Zobel, D., Krane, H.-G., Morgenroth, W. & Luger, P. (1998). *Science*, **279**, 356–358.
Koritsanszky, T., Howard, S., Su, Z., Mallinson, P. R., Richter, T. & Hansen, N. K. (1997). *XD – a Computer Program Package for Multipole Refinement and Analysis of Electron Densities from Diffraction Data.* Free University of Berlin, Berlin, Germany.
Lee, C., Yang, W. & Parr, R. G. (1988). *Phys. Rev. B*, **37**, 785–789.
Møller, C. & Plesset, M. S. (1934). *Phys. Rev.* **46**, 618–622.
Monkhorst, H. J. & Pack, J. D. (1976). *Phys. Rev. B*, **13**, 5188–5192.
Ojamae, L., Hermansson, K., Dovesi, R., Roetti, C. & Saunders, V. R. J. (1994). *J. Chem. Phys.* **100**, 2128–2138.
Pérès, N., Boukhris, A., Souhassou, M., Gavoille, G. & Lecomte, C. (1999). *Acta Cryst.* A**55**, 1038–1048.
Platts, J. A. & Howard, S. T. (1996). *J. Chem. Phys.* **11**, 4668–4674.
Saunders, V. R., Dovesi, R., Roetti, C., Causà, M., Harrison, N. M., Orlando, R. & Zicovich-Wilson, C. M. (1998). *CRYSTAL98 User's Manual.* University of Torino, Torino, Italy.
Stewart, R. F. (1976). *Acta Cryst.* A**32**, 565–574.
Stewart, R. F. J. (1969). *J. Chem. Phys.* **51**, 4569–4577.
Towler, M. D. (1999). Private communication.
Volkov, A., Abramov, Yu. & Coppens, C. (2000). In preparation.
Volkov, A. & Coppens, P. (2000). In preparation.
Volkov, A., Gatti, C., Abramov, Y. & Coppens, P. (2000). *Acta Cryst.* A**56**, 252–258.
Volkov, A., Wu, G. & Coppens, P. (1999). *J. Synchrotron Rad.* **6**, 1007–1015.
Woon, D. E. & Dunning, T. H. Jr (1993). *J. Chem. Phys*. **98**, 1358–1373.
Zhang, Y. & Coppens, P. (1999). *Chem. Commun.* **23**, 2425–2426.